

New Bithiazole-Based Sensitizers for Efficient and Stable Dye-Sensitized Solar Cells

Jinxiang He, Fuling Guo, Xin Li, Wenjun Wu,* Jiabao Yang, and Jianli Hua*^[a]

Abstract: A series of new push–pull organic dyes (**BT-I–VI**), incorporating electron-withdrawing bithiazole with a thiophene, furan, benzene, or cyano moiety, as π spacer have been synthesized, characterized, and used as the sensitizers for dye-sensitized solar cells (DSSCs). In comparison with the model compound **T1**, these dyes containing a thiophene moiety between triphenylamine and bithiazole display enhanced spectral responses in the red portion of the solar spectrum. Electrochemical measurement data indicate that the HOMO and LUMO energy levels can be tuned by introducing different π spacers between the bithiazole

moiety and cyanoacrylic acid acceptor. The incorporation of bithiazole substituted with two hexyl groups is highly beneficial to prevent close π – π aggregation, thus favorably suppressing charge recombination and intermolecular interaction. The overall conversion efficiencies of DSSCs based on bithiazole dyes are in the range of 3.58 to 7.51%, in which **BT-I**-based DSSCs showed the best photovoltaic performance: a maximum monochromatic inci-

dent photon-to-current conversion efficiency (IPCE) of 81.1%, a short-circuit photocurrent density (J_{sc}) of 15.69 mA cm⁻², an open-circuit photovoltage (V_{oc}) of 778 mV, and a fill factor (ff) of 0.61, which correspond to an overall conversion efficiency of 7.51% under standard global AM 1.5 solar light conditions. Most importantly, long-term stability of the **BT-I–III**-based DSSCs with ionic-liquid electrolytes under 1000 h of light soaking was demonstrated and **BT-II** with a furan moiety exhibited better photovoltaic performance of up to 5.75% power conversion efficiency.

Keywords: bithiazoles • dyes/pigments • photophysics • sensitizers • solar cells

Introduction

Converting solar energy into electricity is generally considered to be the most promising way to solve the energy crisis in the whole world. A variety of light-harvesting devices were developed rapidly including dye-sensitized solar cells (DSSCs),^[1] which have attracted great worldwide attention. As potential candidates for the future modality of photovoltaic cells, DSSCs manifest considerable efficiency and low cost, in which the sensitizer is deemed to be the crucial component. At present, DSSC sensitizers based on Ru^{II}-polypyridyl complexes have achieved power conversion efficiencies of almost 12% at standard global air mass (AM) 1.5.^[2] However, the large-scale application of Ru complexes has become a critical problem due to limited resources and the hefty purification steps needed.^[3] In recent years, the interest in organic dyes as substitutes of noble metal complexes has been increasing because of their many advantages, such

as large molar extinction coefficient, simple synthesis, low cost, and facile molecular design. Recently, studies have been focused on molecular engineering of chromophores to attain the capability of panchromatic light harvesting. Varieties of organic dyes, such as cyanine,^[4] merocyanine,^[5] coumarin,^[6] indoline,^[7] hemicyanine,^[8] phenothiazine,^[9] phenoxazine,^[10] and diketopyrrolopyrrole or pyrrole dyes,^[11] have been reported, thus making organic dyes fruitful in their application to DSSCs. Impressive photovoltaic performances have been obtained by using organic dyes that show efficiencies exceeding 10%.^[12]

The organic dyes are commonly constructed with donor– π bridge–acceptor (D– π –A)^[13] configurations due to the effective photoinduced intramolecular charge-transfer property. For efficient solar energy conversion, it is desirable to use dyes that possess high molar extinction coefficients that extend throughout the visible into the near-IR regions. As is well known, extending π -conjugated bonding bridges always brings a low stability although it might efficiently redshift the absorption response. Recently, a few organic D–A– π –A dyes incorporating electron-withdrawing terephthalonitrile or electron-deficient heteroarenes, such as quinoline,^[14] isoxazole,^[15] thiazole moieties,^[16] and the pyrimidine ring,^[17] as linkages to cyanoacrylic acid, showed more redshifted absorption than their parent analogues and thus enhanced the light harvesting and stability. Meanwhile, some new D–A– π –A configuration dyes with diketopyrrolopyrrole, bithiazole, and benzothiadiazole moieties have been reported by our

[a] J. He,[†] F. Guo,[†] Dr. X. Li, W. Wu, J. Yang, Prof. Dr. J. Hua
Key Laboratory for Advanced Materials
Institute of Fine Chemicals and Department of Chemistry
East China University of Science and Technology
130 Meilong Road, Shanghai 200237 (P.R. China)
Fax: (+86)21-64252758
Fax: (+86)21-64252756
E-mail: jlhua@ecust.edu.cn
wjwu@ecust.edu.cn

[[†]] These authors contributed equally to this work.

group.^[7d,11a,18] It should be noted that bithiazole is a well-known electron-deficient unit that acts as an acceptor. Two long alkyl chains attached on a thiazole moiety are considered to suppress charge recombination and raise the conduction band edge and hence to acquire a high open-circuit photovoltage (V_{oc}) of DSSCs.^[19] 2-Cyano-3-(5-[5'-[4-(diphenylamino)phenyl]-4,4'-dihexyl-2,2'-bithiazol-5-yl]-4,4'-dihexyl-2,2'-bithiazol-5-yl)thiophen-2-yl)acrylic acid (**T1**; Figure 1) was reported as a dye for efficient DSSCs in our previous studies,^[18] in which we identified that solar cells with bithiazole-based sensitizers could achieve high performance; however, the short-circuit photocurrent density (J_{sc}) for the sensitizer still has room for improvement and optimization. As reported, different π spacers could lead to diverse positions of the HOMO and LUMO energy levels, thus resulting in a different driving force for electron injection and tuning the short-circuit photocurrent density (J_{sc}). To enrich the research field of bithiazole dyes for DSSCs and gain more information on the structure–property relationships, we synthesized six new bithiazole dyes (**BT-I–VI**, Figure 1).

For **BT-I–III**, we added a thiophene moiety between triphenylamine and bithiazole to extend the absorption wavelength and improve the molar extinction coefficient (ϵ).^[6a] At present most of the metal-free dye sensitizers with high efficiency rely on thiophene or thiophene-based heterocycles as the π spacer. Furan, thiophene's oxygen analogue,

which has a smaller resonance energy (16 kcal mol⁻¹) in the spacer than the thiophene (29 kcal mol⁻¹) and benzene (36 kcal mol⁻¹), would be more efficient for the hole location and reinforce the stability of the dye sensitizers.^[20] Also, some reports have shown that incorporation of a furan moiety could somewhat improve the solubility of the organic dyes.^[21] In addition, we also synthesized bithiazole-based sensitizers containing a cyano moiety (**BT-IV–VI**). The cyanovinyl group can improve the energy gap of dyes to increase the absorption wavelength for better light harvesting. A cyanovinyl unit can effectively stabilize the LUMO level and shift the electronic absorption band.^[22] Finally, the six sensitizers were applied to the sensitization of nanocrystalline TiO₂-based solar cells, and the effect of π -spacer linkers on the photophysical and electrochemical properties of the dyes and the solar cell performance are detailed.

Results and Discussion

Synthesis: The synthetic route to the six dyes (**BT-I–VI**) containing the bithiazole moiety is depicted in Scheme 1. As is well known, the strong intermolecular π – π interaction may lead to interfacial charge recombination, thus resulting in a decrease in V_{oc} . The two long hexyl groups on the bithiazole unit can improve the solubility and reduce the inter-

molecular π – π interaction. The Suzuki coupling reaction of 5,5'-dibromo-4,4'-dihexyl-2,2'-bithiazole with thiophen-2-ylboronic acid afforded the monosubstituted compound **1**. The reaction produced the disubstituted side products as well; fortunately monosubstituted compounds can be easily separated by column chromatography. In the next step, the Suzuki coupling reaction of **1** with 5-formylthiophen-2-ylboronic acid, 5-formylfuran-2-ylboronic acid, and 4-formylphenylboronic acid afforded compounds **2–4**, respectively. Then, the reactions of compounds **5–7** with 4-(diphenylamino)phenylboronic acid provided aldehyde precursors **8–10**, respectively. As depicted in Scheme 1, the syntheses of the important intermediates **14–16** were also started from 5,5'-dibromo-4,4'-dihexyl-2,2'-bithiazole. The asymmetrical Suzuki coupling with 4-(diphenylamino)phenylboronic acid afforded monosubstituted compound **11**, and then com-

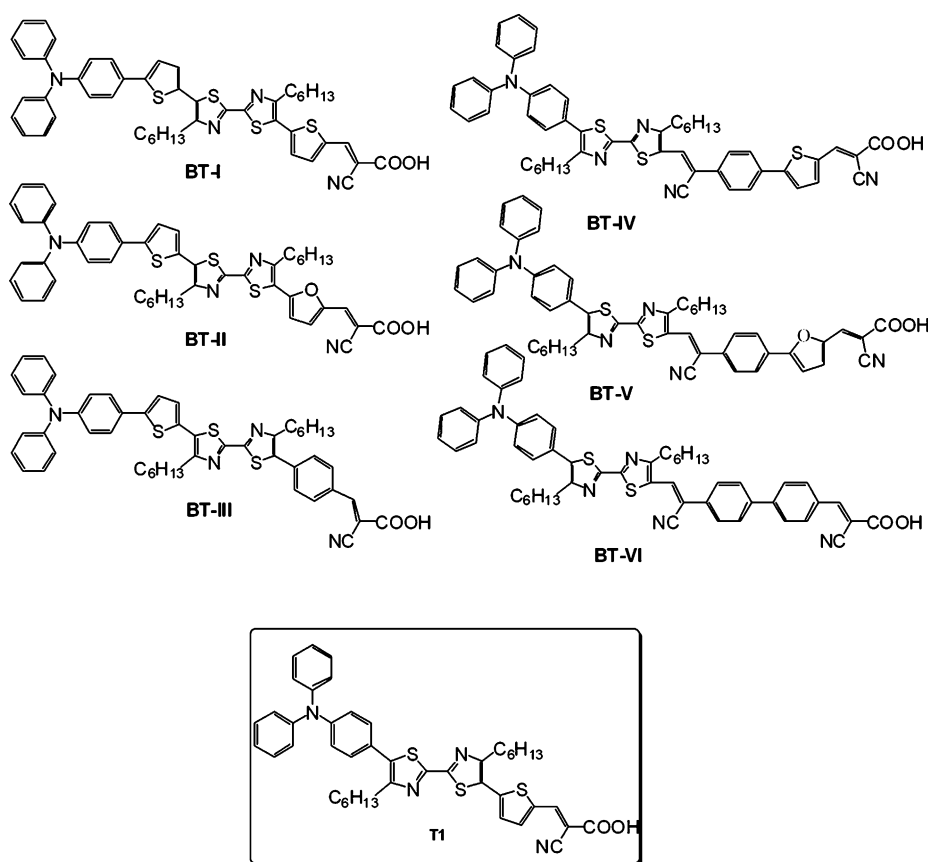
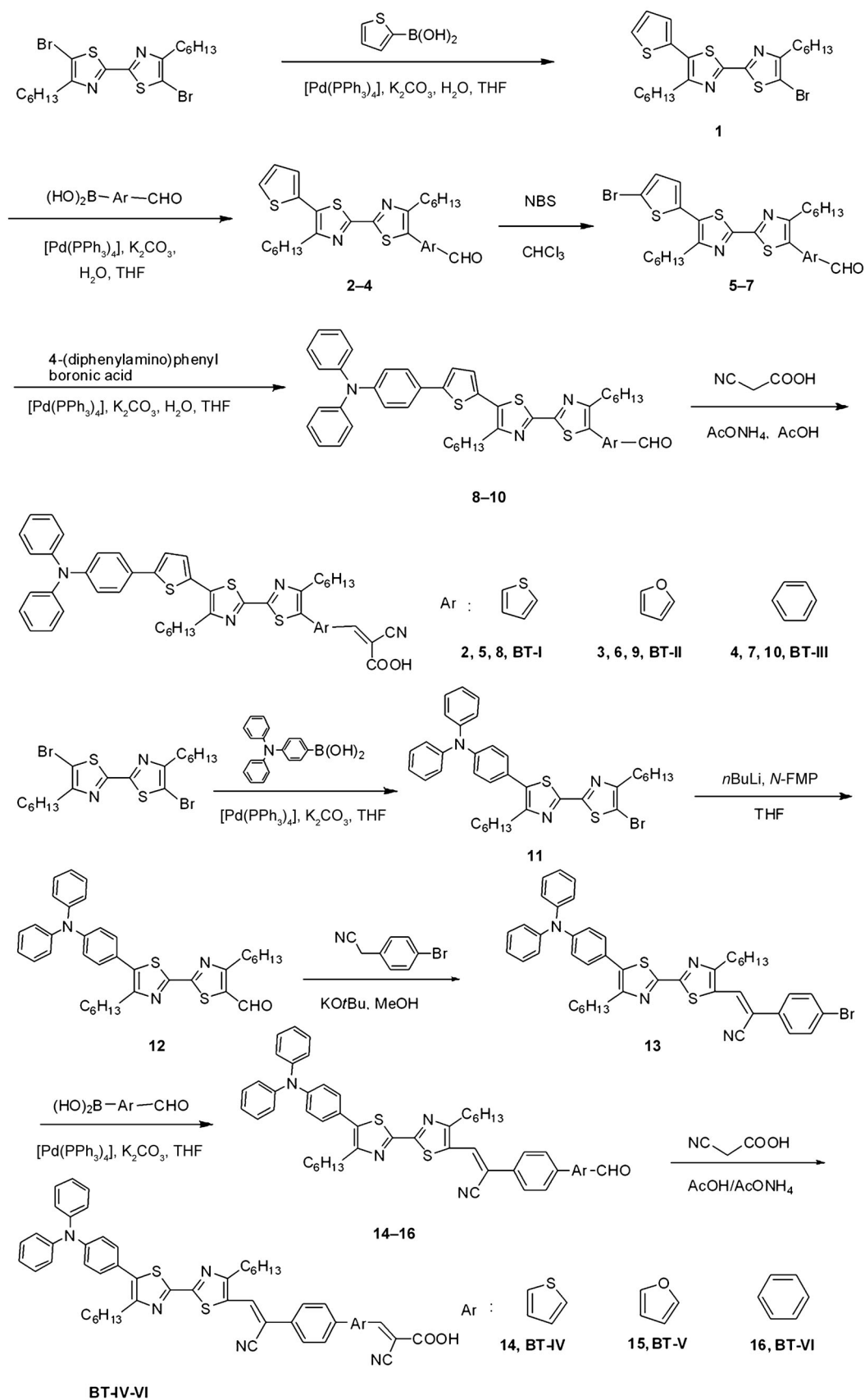


Figure 1. Chemical structures of the sensitizers (**BT-I–VI**) and the reference dye **T1**.

Scheme 1. Synthetic routes to bithiazole-based dyes **BT-I-VI**. NBS = *N*-bromosuccinimide, *N*-FMP = *N*-formylmorpholine.

pound **12** was obtained by bromoformylation of **11**. The Knoevenagel condensation reaction of **12** with 2-(4-bromophenyl)acetonitrile afforded **13**, in which the Suzuki coupling reaction of **13** with 5-formylthiophen-2-ylboronic acid, 5-formylfuran-2-ylboronic acid, and 4-formyl phenylboronic acid afforded precursors **14–16**, respectively. Finally, the target products (**BT-I–VI**) were synthesized by the Knoevenagel condensation reaction of aldehydes **8–10** and **14–16** with cyanoacetic acid in the presence of acetic acid and ammonium acetate. All the key intermediates and six new organic bithiazole-based sensitizers (**BT-I–VI**) were confirmed by ^1H and ^{13}C NMR spectroscopy and HRMS.

Absorption properties in solution and on TiO₂ film: The UV/Vis absorption spectra in dichloromethane and adsorbed onto 5 μm transparent TiO₂ films of the dyes **BT-I–VI** and **T1** are shown in Figure 2 and the corresponding data are summarized in Table 1. In the UV/Vis spectra, these new dyes exhibit three major bands at 280–325, 340–360, and 420–550 nm, respectively. The absorption band at 280–325 nm was ascribed to a localized aromatic $\pi\text{--}\pi^*$ transition typical of triphenylamine, and the middle weak shoulder peak was due to the $\pi\text{--}\pi^*$ transition of triphenylamine and the thiophene moiety for **BT-I–III**. The three dyes containing a cyano moiety exhibit no obvious peak in the 340–360 nm range. The prominent bands at around 420–550 nm can be attributed to the intramolecular charge transfer

Table 1. Optical and electrochemical properties of bithiazole dyes **BT-I–VI** and **T1**.

Dye	$\lambda_{\text{max}}^{[\text{a}]}$ [nm] (ϵ [$10^{-4}\text{M}^{-1}\text{cm}^{-1}$])	$\lambda_{\text{max}}^{[\text{b}]}$ [nm]	HOMO ^[c] [V] (vs. NHE)	$E_{0-0}^{[\text{d}]}$ [eV]	LUMO ^[e] [V] (vs. NHE)
BT-I	470 (4.07)	483	1.10	2.12	-1.02
BT-II	475 (3.84)	512	1.12	2.16	-1.04
BT-III	433 (3.65)	434	1.13	2.34	-1.20
BT-IV	471 (5.02)	540	1.27	2.19	-0.92
BT-V	480 (4.13)	534	1.28	2.21	-0.93
BT-VI	459 (4.40)	517	1.31	2.28	-0.97
T1	457 (3.44)	471	1.06	2.42	-1.36

[a] Absorption maximum in CH_2Cl_2 . [b] Absorption maximum on TiO₂ film. [c] HOMOs were measured in THF with 0.1 M tetrabutylammonium hexafluorophosphate (TBAPF₆) as the electrolyte (working electrode: Pt; reference electrode: SCE; calibrated with ferrocene/ferrocenium (Fc/Fc⁺) as an external reference; counter electrode: Pt wire). [d] E_{0-0} was estimated from the absorption spectrum in solution. [e] LUMO is estimated by subtracting E_{0-0} from the HOMO.

(ICT) between the triphenylamine donor and the acceptor. For the charge-transfer band, the absorption maxima in CH_2Cl_2 are at 470, 475, and 433 nm for **BT-I–III**, and 471, 480, 459, and 457 nm for **BT-IV–VI** and **T1**, respectively. Except for **BT-III**, the other five dyes exhibit slightly redshifted absorption compared with that of dye **T1** due to the extended conjugated structure.

For the three dyes containing a thiophene moiety between triphenylamine and bithiazole, **BT-I** and **BT-II** have very similar absorption properties. Compared with **BT-I** and **BT-II**, **BT-III** exhibits about a 40 nm blueshift in absorption. This may be caused by the decrease of coplanarity between the bithiazole moiety and the electron acceptor due to the introduction of the benzene unit. Meanwhile, similar phenomena were observed for the dyes with a cyano moiety (**BT-IV–VI**), in which **BT-VI** exhibits about a 12 and 21 nm blueshift in absorption relative to **BT-IV** and **BT-V**, respectively.

From the optimized ground-state geometries shown in Table 2, the dihedral angles between the bithiazole rings and π spacer near the anchoring moiety are predicted to be 0.6, 0.1, 34.8, 22, 0.5, 34.2, and 0.2° for **BT-I–VI** and **T1**, respectively. The relatively large dihedral angles for phenylene-bridged **BT-III** and **BT-VI** lead to a large blueshift of absorption in solution. The torsion angle for furan-bridged **BT-II** is a little smaller than that for thiophene-bridged **BT-I**, which results in a 5 nm redshifted absorption. Meanwhile **BT-V** exhibits about a 9 nm redshift in absorption compared to **BT-VI**.

The molar extinction coefficients (ϵ_{max}) of **BT-I–VI** and **T1** are 40700, 38400, 36500, 50200, 41300, 44000, and 34400 $\text{M}^{-1}\text{cm}^{-1}$, respectively, in which the **BT-I–VI** dyes have a higher molar extinction coefficient than the corresponding dye **T1** and the ϵ_{max} of **BT-IV–VI** is higher than those of **BT-I–III**, respectively, thus suggesting that **BT-IV–VI** can harvest sunlight more effectively. In comparison with conventional ruthenium complexes (for example, $1.39 \times 10^4 \text{M}^{-1}\text{cm}^{-1}$ for N719),^[23] the greater maximum absorption coefficients of the organic dyes allow a correspondingly thinner nano-

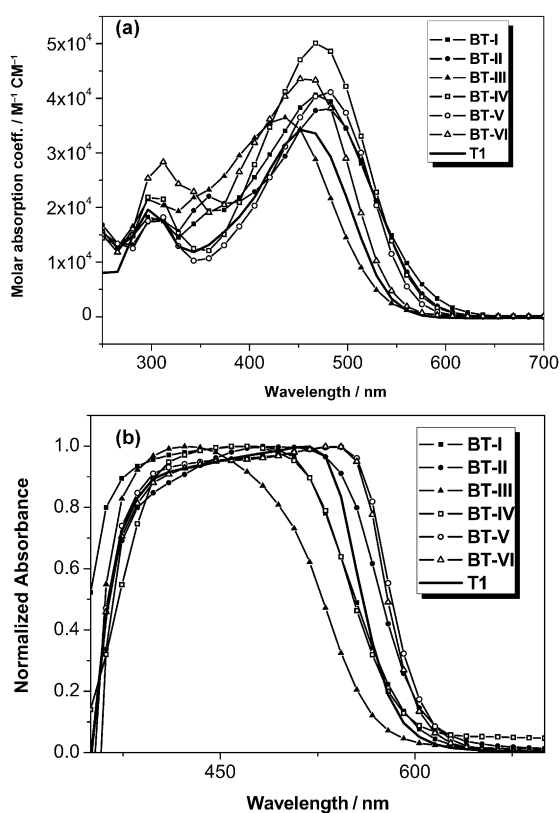
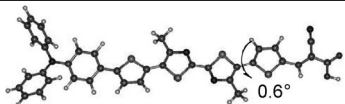
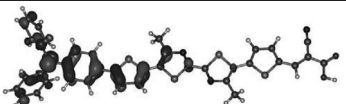
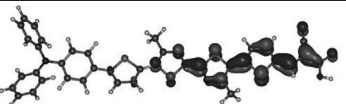
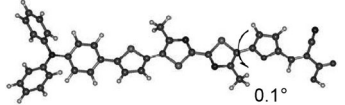
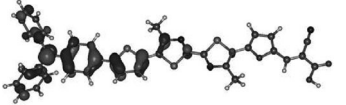
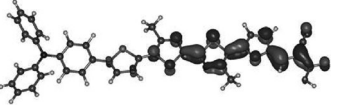
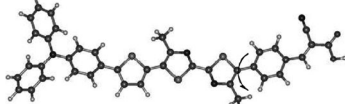
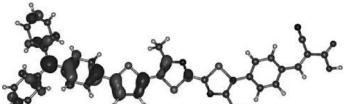
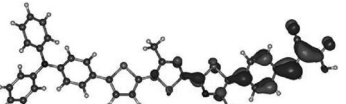
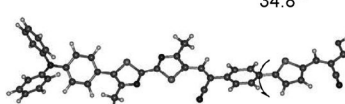
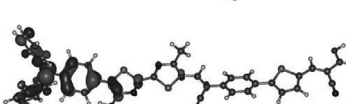
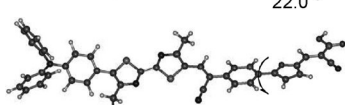
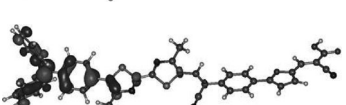
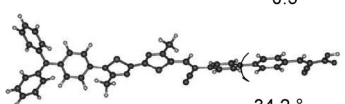
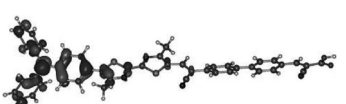
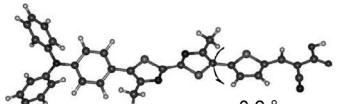
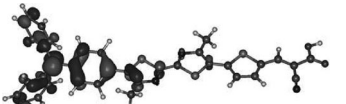


Figure 2. Absorption spectra of **BT-I–VI** and **T1**, measured a) in CH_2Cl_2 and b) adsorbed onto 5 μm transparent TiO₂ films.

Table 2. Optimized structures and electron distribution in HOMO and LUMO levels of the **BT** dyes.

Dye	Optimized structure ^[a]	HOMO	LUMO
BT-I	 0.6°		
BT-II	 0.1°		
BT-III	 34.8°		
BT-IV	 22.0°		
BT-V	 0.5°		
BT-VI	 34.2°		
T1	 0.2°		

[a] The dihedral angles between the bithiazole rings and π spacer near the anchoring moiety are given in the graphics.

crystalline film, thereby avoiding a decrease in the film's mechanical strength. This also benefits the electrolyte diffusion in the film and reduces the recombination possibility of the light-induced charges during transportation.^[4c,24]

Compared to the spectrum in CH_2Cl_2 solution, the absorption peaks for **BT-I–VI** and **T1** on $5\ \mu\text{m}$ transparent TiO_2 film are all redshifted (Table 1). Generally, when sensitizers are anchored onto a nanocrystalline TiO_2 surface, they have a strong tendency to aggregate in solution or at the solid/liquid interface due to a strong attractive force between the molecules. Dye aggregates usually have three forms: redshifted J-aggregates, blueshifted H-aggregates, and both red- and blueshifted herringbone aggregates. From the above, all of the dyes have strong J-aggregates. In particular, **BT-IV–VI** have much stronger aggregation than the dyes **BT-I–III** without a cyano moiety (see Figure 2). Also, the experimental results indicate that the bithiazole-based dyes used in this work form J-aggregates on the TiO_2 nanocrystal surface. The interaction between the carboxylate group and the surface Ti^{4+} ions may lead to increased delocalization of the π^* orbital of the conjugated framework. The energy of the π^* level is decreased by this delocalization, which explains the redshift of the absorption spectra. It is noteworthy that the absorption spectra of dyes adsorbed

onto transparent TiO_2 show a markedly broad profile, which is beneficial to light harvesting.

Electrochemical properties: To evaluate the possibility of electron transfer from the excited dye to the conduction band of TiO_2 , cyclic voltammetry was performed in tetrahydrofuran, with 0.1 M tetrabutylammonium hexafluorophosphate as the supporting electrolyte, Pt as the working electrode and counter electrode, and a saturated calomel electrode (SCE) as the reference electrode. The examined HOMO and LUMO levels are collected in Table 1. The SCE reference electrode was calibrated by using a ferrocene/ferrocenium (Fc/Fc^+) redox couple as an external standard and the $E_{1/2}$ of the Fc/Fc^+ redox couple was found to be 0.55 V versus the SCE reference electrode. The potentials versus the normal hydrogen electrode (NHE) were calibrated by addition of 0.63 V to the potentials versus Fc/Fc^+ .^[9a] Therefore, the potentials measured versus the SCE were converted to NHE by addition of 0.08 V. It can be seen from Figure 3 that the first half-wave potentials of the dyes **BT-I–VI** are 1.02, 1.04, 1.05, 1.19, 1.20, and 1.23 V (vs. SCE), respectively. Therefore, the ground-state oxidation potential corresponding to the HOMO levels are 1.10, 1.12, 1.13, 1.27, 1.28, and 1.31 V (vs. NHE), respectively. The bandgap energies (E_{0-0}) of the six dyes were 2.12, 2.16, 2.34,

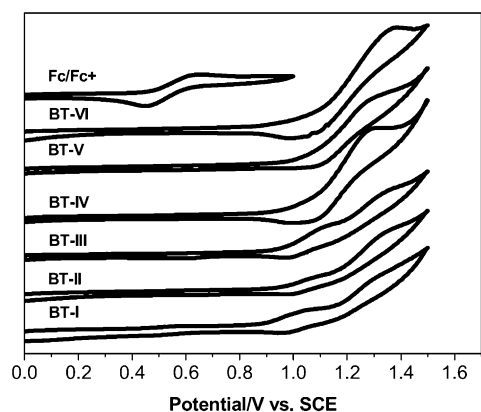


Figure 3. Cyclic voltammograms of bithiazole dyes **BT-I–VI** measured in THF with TBAPF₆ (0.1 M) as the electrolyte.

2.19, 2.21, and 2.28 eV, respectively, which were estimated from the absorption thresholds from absorption spectra in solution. The estimated excited-state potential corresponding to the LUMO levels, calculated from $E_{\text{HOMO}} - E_{0-0}$, are -1.02 , -1.04 , -1.20 , -0.92 , -0.93 , and -0.97 V, respectively. It is clear that the HOMO energy level of **T1** is higher than those of **BT-I–VI**. At the same time, introduction of a thiophene unit between triphenylamine and bithiazole elevates the HOMO levels. Based on Figures 3 and 4, **BT-IV–VI** are

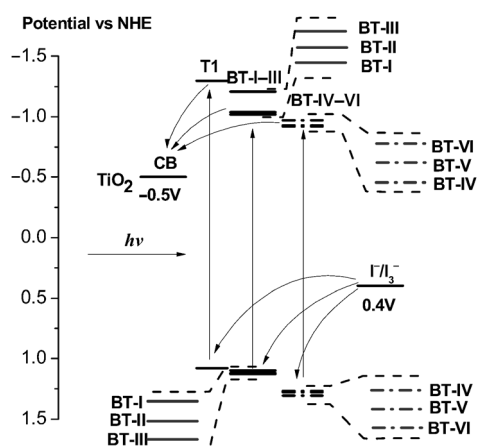


Figure 4. Experimental energy-level diagrams of the HOMO and LUMO for **BT-I–VI** and **T1** versus SCE. The dashed lines show the relative positions of the energy levels of dyes. CB = conduction band.

oxidized at more positive potentials than **BT-I–III**. On the other hand, the introduction of the cyano group into **BT-IV–VI** lowers their LUMO energy level by increasing the electron affinity.

From these data, we found that the HOMO levels of the dyes are much more positive than the iodine/iodide redox potential value (0.4 V), thus, indicating that the oxidized dyes, formed after electron injection into the conduction band of TiO₂, could accept electrons from I⁻ ions thermodynamically (see Figure 4). The LUMO levels of these dyes

are considerably more negative than the conduction-band-edge energy level (E_{cb}) of the TiO₂ electrode (-0.5 V vs. NHE), which implies that electron injection from the excited dye into the conduction band of TiO₂ is energetically permitted.^[25] The relatively large energy gaps between the LUMO and E_{cb} provide the possibility for the addition of 4-*tert*-butylpyridine (TBP) to the electrolyte, which can shift the E_{cb} of TiO₂ more negatively and, consequently, improve the voltage and total efficiency.^[26]

To gain better insight into the electronic properties of these dyes, density functional theory (DFT) calculations were performed at the B3LYP/6-31G* level. The electron distribution of the HOMOs and LUMOs of bithiazole dyes are shown in Table 2. The electron density of the HOMOs of **BT-I–VI** and **T1** sensitizers are primarily located at triphenylamine, whereas those of the LUMOs are delocalized over the aromatic rings, thiophene, furan, and benzene moieties, and the anchoring group. In particular, the electron density of the LUMOs is located at the electron trap of cyano vinyl units for the dyes with a cyano moiety. This leads to inefficient electron injection. The electron density on the anchoring group also suggests that the excitation from the HOMO to the LUMO can move the electron distribution from the triphenylamine donor unit to the cyanoacrylic acid anchoring moiety to realize electron injection into the conduction band of TiO₂.

Photovoltaic device performance: Figure 5 shows the action spectra of incident photon-to-current conversion efficiency (IPCE) for DSSCs based on these dyes. The dye-coated TiO₂ film was used as the working electrode, platinumized fluorine-doped tin oxide (FTO) glass as the counter electrode, and 0.6 M 1,2-dimethyl-3-*n*-propylimidazolium iodide (DMPII), 0.05 M I₂, 0.10 M LiI, and 0.5 M TBP in acetonitrile and methoxypropionitrile (volume ratio, 7:3) mixed solution as the redox electrolyte. Generally, the solar cells sensitized by **BT-I–III** have better performances than the dyes with a

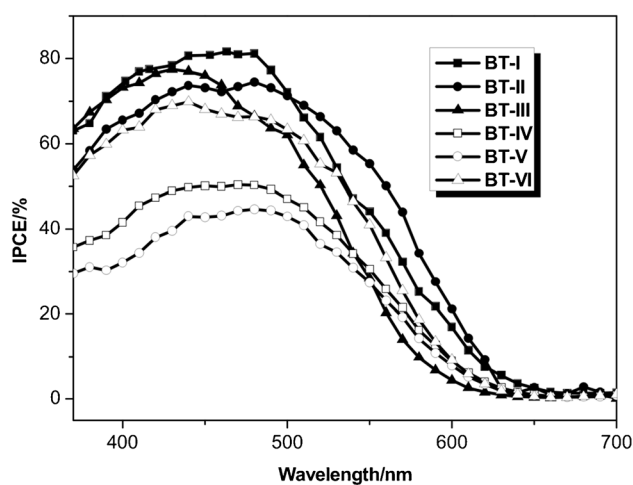


Figure 5. Photocurrent action spectra of the TiO₂ electrodes sensitized by **BT-I–VI**.

cyano moiety in the range of 370–500 nm, especially for **BT-IV–VI** in the range of 370–630 nm. These results can be ascribed to the more negative LUMO energy level of **BT-I–III** leading to higher electron-injection efficiency. The solar cells based on **BT-I** and **BT-III** exhibit high IPCE values above 60% in the range of 400–500 nm and with a highest value of 81.1% at 480 nm for **BT-I**, and 76.9% at 440 nm for **BT-III**. The **BT-II**- and **BT-VI**-sensitized cells have IPCE values above 55% in the range of 370–520 nm, whereas the IPCE value of **BT-IV** and **BT-V** are reduced significantly. This leads to the poor performance of the **BT-IV**- and **BT-V**-based DSSCs in terms of photovoltage efficiency. The threshold wavelengths of the IPCE spectra for all of the dyes were located below 640 nm, especially for **BT-III** at about 600 nm, which is consistent with the absorption spectra when dyes were adsorbed onto TiO₂ films. Figure 6

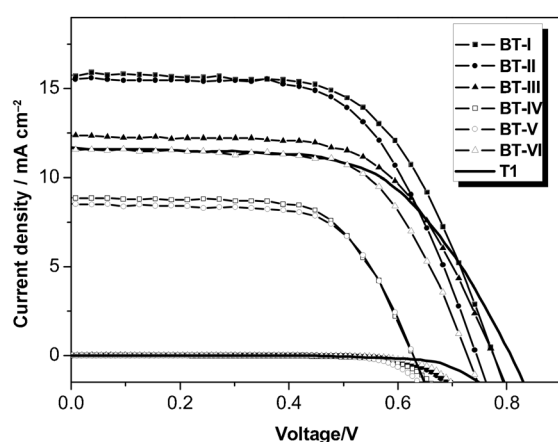


Figure 6. Current–voltage characteristics of DSSCs sensitized by the dyes **BT-I–VI** and **T1** under irradiation of AM 1.5G simulated solar light (100 mW cm⁻²) with liquid electrolyte.

shows the current–voltage characteristics of DSSCs fabricated with these bithiazole dyes (**BT-I–VI** and **T1**) as sensitizers under standard global AM 1.5 solar light conditions. The detailed parameters of short-circuit current density (J_{sc}), open-circuit voltage (V_{oc}), fill factor (ff), and photovoltaic conversion efficiency (η) are summarized in Table 3.

Table 3. Photovoltaic performance of DSSCs based on the dyes **BT-I–VI** and **T1** with a liquid electrolyte.^[a]

Dye	J_{sc} [mA cm ⁻²]	V_{oc} [mV]	ff	η [%]
BT-I	15.69	778	0.61	7.51
BT-II	15.42	748	0.62	7.11
BT-III	12.47	789	0.61	6.01
BT-IV	8.95	625	0.66	3.69
BT-V	8.43	623	0.68	3.58
BT-VI	11.54	728	0.65	5.49
T1	11.78	810	0.60	5.73

[a] Illumination: 100 mW cm⁻² simulated AM 1.5G solar light; electrolyte containing: 0.1 M LiI, 0.05 M I₂, 0.6 M DMPII, and 0.5 M TBP in the mixed solvent of acetonitrile and 3-methoxypropionitrile (7:3, v/v).

The short-circuit current J_{sc} is related to the molar extinction coefficient of the dye molecule, for which a higher molar extinction coefficient yields a higher short-circuit current. The onset wavelengths of **BT-I** and **BT-II** are redshifted by 50 and 40 nm with respect to **T1** in solution, respectively. The molar extinction coefficient of **BT-I–III** is higher than that of **T1**, in which **BT-I** has the largest ϵ_{max} . Compared with **T1**, **BT-I–III** have an increased light-harvesting efficiency and consequently improved J_{sc} due to their higher molar extinction coefficients and broader photocurrent action spectra. In addition, the open-circuit photovoltage of **BT-III** is better than those of **BT-I** and **BT-II**-based solar cells. This may be caused by the introduction of benzene, which leads to reduction of electron recombination. Consistent with the results of IPCE, the photovoltaic data of **BT-I** and **BT-II** are superior to those of **BT-III**. Different from **BT-I–III**, the dyes **BT-IV–VI** linked by the cyanovinyl unit perform with relatively lower photovoltage efficiency. There is no improvement of the device efficiency, although incorporation of the cyano moiety in the conjugated bridge leads to bathochromic and hyperchromic shifts for light harvesting. This outcome may be comprehended in that the charge-trapping effect of the internal electron-withdrawing character of the cyanovinyl unit hampers electron injection from the excited sensitizers into TiO₂, suggested by the low J_{sc} values of DSSCs in this study.^[22] Similar to **BT-I–III**, **BT-VI** connected by the benzene ring for **BT-IV–VI** performs with the best V_{oc} and leads to much better performance than **BT-IV** and **BT-V**. This phenomenon can be understood by the fact that the **BT-VI**-based cell shows much higher IPCE values between 370 and 560 nm than **BT-IV**- and **BT-V**-based cells. On the other hand, from the absorption spectra of dyes adsorbed onto TiO₂ films, **BT-IV** and **BT-V** have similar large-scale absorption peaks. These two dyes exhibit greater aggregation, which is not of benefit to light-to-current conversion.

Overall, the **BT-I–III**-sensitized cell gave a J_{sc} of 15.69, 15.42, and 12.47 mA cm⁻², a V_{oc} of 778, 748, and 789 mV, and a ff of 0.61, 0.62, and 0.61, corresponding to an overall conversion efficiency of 7.51, 7.11, and 6.01%, respectively. Under the same conditions, the photovoltaic parameters (J_{sc} , V_{oc} , ff, and η) of cells sensitized by **BT-IV–VI** are: 8.95 mA cm⁻², 625 mV, 0.66, and 3.69%; 8.43 mA cm⁻², 623 mV, 0.68, and 3.58%; and 11.54 mA cm⁻², 728 mV, 0.65, and 5.49%, respectively. It was found that the V_{oc} value of **BT-III** is 11 mV higher than those of **BT-I** and **BT-II**, and of **BT-VI** is 103 mV higher than those of **BT-IV** and **BT-V**, thus indicating that the charge recombination process was effectively retarded by introducing benzene as the π spacer.

We also measured the photovoltaic performance of **BT-IV**- and **BT-V**-based DSSCs with co-adsorbent (chenodeoxycholic acid) for comparison, and they exhibited conversion efficiencies of 3.83 and 3.79%, respectively. Therefore, co-adsorbents have less impact on improving the photovoltaic performance of DSSCs based on the two dyes. To understand why **T1** has the largest open-circuit voltage, the effect of **BT-I–VI** and **T1** on dark current was studied as shown in

Figure 6. It is clear that the **T1** dark-current onset potential shifted to a larger value than that of **BT-I–VI**. This dark-current change indicates that **T1** can inhibit charge recombination between injected electrons and I_3^- ions in the electrolyte.

Electrochemical impedance spectroscopy: In addition, electrochemical impedance spectroscopy (EIS) was employed to study the electron recombination in DSSCs based on these **BT-I–VI** dyes under -0.70 V bias applied voltage in the dark. The Nyquist plot, Bode plot, and equivalent circuit are shown in Figure 7 a–c, respectively. Some important parameters can be obtained by fitting the EIS data with an electro-

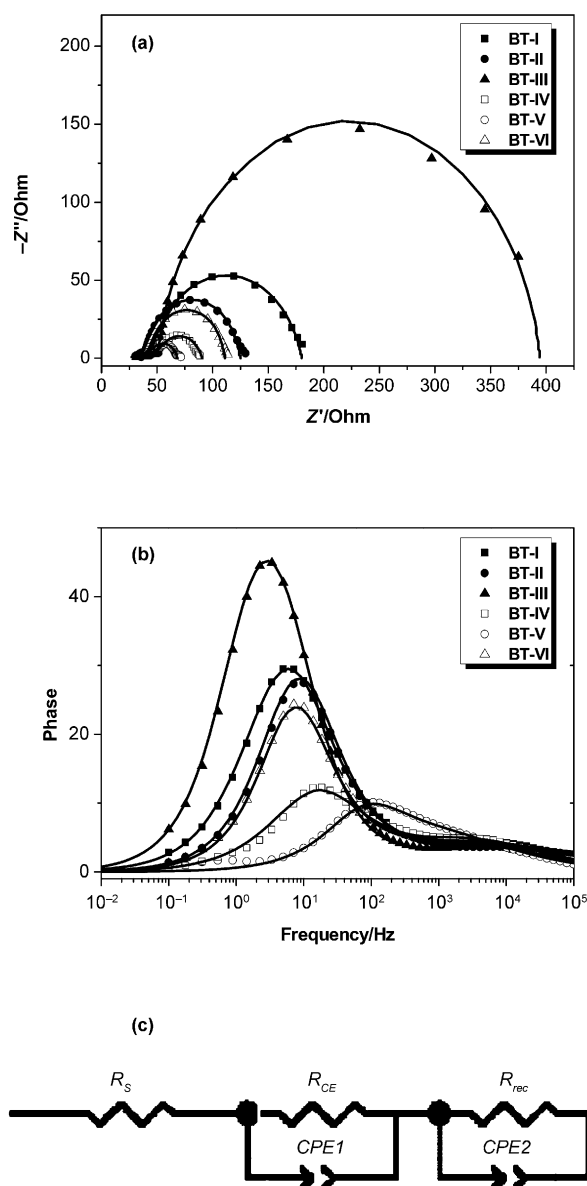


Figure 7. Impedance spectra for DSSCs based on dyes **BT-I–VI** measured at -0.70 V bias in the dark. a) Nyquist plots; b) Bode phase plots; c) equivalent circuits. The lines in (a) and (b) show theoretical fits by using the equivalent circuits in (c). CPE = constant phase element (in EIS circuit).

chemical model.^[27] In Figure 7 c, R_s , R_{rec} , and R_{CE} represent series resistance and charge-transfer resistances at the dye/ TiO_2 /electrolyte interface and counter electrode (CE), respectively. The series resistance (R_s) and electrolyte reduction resistance (R_{CE}) corresponding to the first semicircle in Figure 7 a show almost the same value in the six dye-based DSSCs due to the same electrode material and same electrolyte, and the R_{rec} corresponds to the middle semicircle. From the EIS measurements, the electron lifetime (τ_e) expressing the electron recombination between the electrolyte and TiO_2 was calculated following a literature procedure.^[28] The reaction resistance of the DSSCs consisting of TiO_2 /dye/electrolyte and Pt/electrolyte interfaces based on **BT-I–VI** were analyzed by software (ZSimpWin) using an equivalent circuit. As shown in Table 4, the R_{rec} of the **BT-I–VI** dyes

Table 4. Parameters obtained by fitting the impedance spectra of the DSSCs with sensitizers by using the equivalent circuit (Figure 7c).

Dye	R_s [Ω]	R_{CE} [Ω]	R_{rec} [Ω]	τ_e [ms]
BT-I	31.6	14.0	134.6	62.2
BT-II	27.6	14.9	84.6	35.9
BT-III	39.4	11.8	343.0	169.7
BT-IV	36.6	18.0	32.5	13.1
BT-V	35.2	14.8	18.4	2.4
BT-VI	29.4	17.3	64.7	34.5

are 134.6, 84.6, 343.0, 32.5, 18.4, and 64.7 Ω , respectively. The electron lifetimes of the **BT-I–VI** dyes are 62.2, 35.9, 169.7, 13.1, 2.4, and 34.5 ms, respectively. Dye **BT-III** gives the longest τ_e among these dyes. A dye with a longer lifetime can avoid electron recombination efficiently and has a better V_{oc} . This result is in agreement with the observed shift in the V_{oc} value under standard global AM 1.5 illumination.

Performance of a solvent-free solar cell and its stability:

Long-term stability is a vital parameter for sustained cell operation, so we substituted the liquid electrolyte with a solvent-free ionic liquid. Bithiazole dyes **BT-I–III** were evaluated as sensitizers for the solvent-free ionic liquid electrolyte DSSC with 0.1 M iodine, 0.1 M lithium iodide, and 0.45 M benzimidazole in 1-propyl-3-methylimidazolium iodide as redox electrolyte, because the DSSCs employing dyes **BT-I–III** showed a better photovoltaic performance than those with **BT-IV–VI**. The photovoltaic performances of the **BT-I–III**-sensitized TiO_2 film electrodes with an ionic liquid electrolyte are listed in Table 5 under standard global AM 1.5 solar light conditions (100 mW cm^{-2}), and the corresponding photocurrent–voltage curves are shown in Figure 8. The **BT-I–III**-sensitized cells gave J_{sc} values of 13.87, 13.80, and 12.00 mA cm^{-2} , V_{oc} values of 0.633, 0.641, and 0.676 V, and ff values of 0.63, 0.65, and 0.64, corresponding to η values of 5.49, 5.75, and 5.22 %, respectively. The η value of **BT-II** is higher than that of **BT-I** in a solvent-free ionic-liquid electrolyte, which is the opposite result to that in a liquid electrolyte for **BT-I** and **BT-II**. This could be explained by the

Table 5. Performance parameters of solvent-free ionic-liquid electrolyte solar cells sensitized by **BT-I-III**.^[a]

Dye	J_{sc} [mA cm^{-2}]	V_{oc} [mV]	ff	η [%]
BT-I	13.87	633	0.63	5.49
BT-II	13.80	641	0.65	5.75
BT-III	12.00	676	0.64	5.22

[a] Illumination: 100 mW cm^{-2} simulated AM 1.5G solar light; electrolyte containing: 0.1 M LiI, 0.05 M I_2 , 0.6 M DMPII, and 0.5 M TBP in the mixed solvent of acetonitrile and 3-methoxypropionitrile (7:3, v/v).

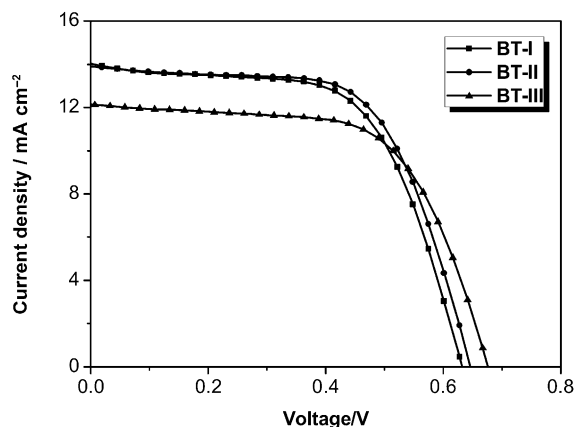


Figure 8. Photocurrent–voltage curves of **BT-I-III**-sensitized TiO_2 electrodes under standard global AM 1.5 illumination (100 mW cm^{-2}) with a solvent-free ionic-liquid electrolyte.

different thickness of TiO_2 films used in the liquid electrolyte and solvent-free ionic-liquid electrolyte DSSCs. The diffusion of I^- and I_3^- ions in an ionic-liquid electrolyte is slow because of their high viscosity, so a thin nanocrystalline TiO_2 film is necessary to reach high conversion efficiencies in solvent-free ionic-liquid electrolyte DSSCs.^[29]

Figure 9 shows the variations of the conversion efficiency of solar cells sensitized with **BT-I-III** under continuous visible-light irradiation (AM 1.5G, 100 mW cm^{-2}). Values for J_{sc} , V_{oc} , ff, and η were recorded over a period of 1000 h. V_{oc} remained almost constant for the first 800 h and then increased gradually. The open-circuit potential for **BT-I-III** increased by 13, 32, and 9 mV, respectively. In contrast to the V_{oc} increase under illumination, all three cells showed an increase in J_{sc} during the initial 400 h, which may be caused by filling of electrolyte into the inner mesopores of the TiO_2 electrode. Upon a continuous 1000 h of light soaking, the photocurrent of the DSSCs based on **BT-I-III** showed an 8.7, 9.0, and 13.3% decrease, respectively. The overall efficiency remained at 90% of the initial value after 1000 h of visible-light soaking. This demonstrates that the amount of dye on the TiO_2 surface remained intact after a long time of light soaking.

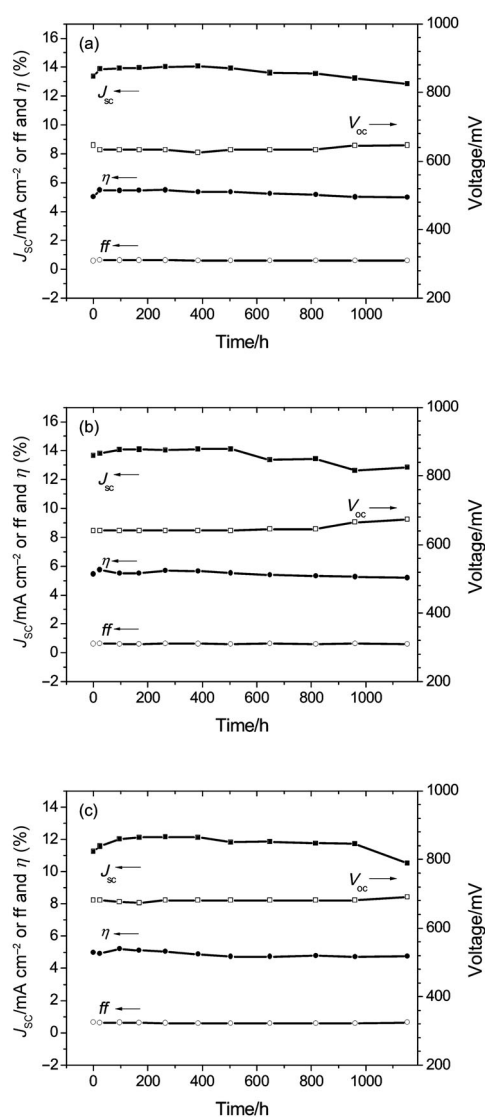


Figure 9. Stability test of photovoltaic parameter (J_{sc} , V_{oc} , ff, and η) variations with aging time for the devices based on a) **BT-I**-, b) **BT-II**-, and c) **BT-III**-sensitized TiO_2 film with a solvent-free ionic-liquid electrolyte during 1 sun visible light irradiation.

Conclusion

Six metal-free organic dyes (**BT-I-VI**), comprising a triphenylamine moiety as the electron donor, a cyanoacrylic acid as the anchoring group, bithiazole substituted with two hexyl groups as the core, and different π spacers, were designed and synthesized for use in DSSCs. The modification of the bithiazole dyes is an effective method to control dye absorption properties, which determines the light-harvesting efficiency. The introduction of a thiophene group between triphenylamine and bithiazole can improve the light-harvesting ability of the dyes. Introduction of a cyano unit can extend the capability for light harvesting of bithiazole, but the charge-trapping effect of the internal electron-withdrawing character of the cyanovinyl unit hampers electron injection into TiO_2 and decreases the device performance.

DSSCs based on **BT-I**, containing a thiophene moiety between triphenylamine and bithiazole, exhibit the best overall light-to-electricity conversion efficiency of 7.51% (J_{sc} = 15.69 mA cm⁻², V_{oc} = 778 mV, ff = 0.61) under AM 1.5 irradiation (100 mW cm⁻²). Most importantly, long-term stability of the **BT-I-III**-based DSSCs with ionic-liquid electrolytes under 1000 h of light soaking was demonstrated, and **BT-II**, with a furan moiety, exhibited a better photovoltaic performance of up to 5.75% power conversion efficiency. All of the results reveal that these metal-free organic bithiazole dyes are promising in the development of DSSCs.

Experimental Section

5-Bromo-4,4'-dihexyl-5'-(thiophen-2-yl)-2,2'-bithiazole (1): 5,5'-Dibromo-4,4'-dihexyl-2,2'-bithiazole (500 mg, 1.02 mmol), [Pd(PPh₃)₄] (20 mg, 0.017 mmol), and K₂CO₃ (1.02 g, 0.01 mol) in THF (10 mL) and H₂O (5 mL) were heated to 45°C under an argon atmosphere for 30 min. A solution of thiophen-2-ylboronic acid (130 mg, 1.02 mmol) in THF (5 mL) was added slowly, and the mixture was heated at reflux for a further 6 h. After cooling to room temperature, THF was evaporated and the mixture was extracted with CH₂Cl₂ (3 × 20 mL). The combined organic layers were dried with anhydrous Na₂SO₄. The solvent was evaporated, and the residue was purified by column chromatography on silica gel (petroleum ether (PE)/CH₂Cl₂ = 10:1–4:1, v/v) to give a yellow solid (450 mg, yield 89%). ¹H NMR (CDCl₃, 400 MHz): δ = 7.38 (d, *J* = 5.2 Hz, 1H), 7.18 (d, *J* = 3.6 Hz, 1H), 7.09 (t, *J* = 4.4 Hz, 1H), 2.91 (t, *J* = 7.8 Hz, 2H), 2.76 (t, *J* = 7.6 Hz, 2H), 1.80–1.68 (m, 4H), 1.43–1.29 (m, 12H), 0.91–0.86 ppm (m, 6H).

5-[4,4'-Dihexyl-5'-(thiophen-2-yl)-2,2'-bithiazol-5-yl]thiophene-2-carbaldehyde (2): Compound **1** (200 mg, 0.40 mmol), [Pd(PPh₃)₄] (20 mg, 0.017 mmol), and K₂CO₃ (1.02 g, 0.01 mol) in THF (10 mL) and H₂O (5 mL) were heated to 45°C under an argon atmosphere for 30 min. A solution of 5-formylthiophen-2-ylboronic acid (126 mg, 0.81 mmol) in THF (5 mL) was added slowly, and the mixture was heated at reflux for a further 2 h. After cooling to room temperature, THF was evaporated and the mixture was extracted with CH₂Cl₂ (3 × 20 mL). The combined organic layers were dried with anhydrous Na₂SO₄. The solvent was evaporated, and the residue was purified by column chromatography on silica gel (PE/CH₂Cl₂ = 3:1–1:1, v/v) to give an orange solid (200 mg, yield 94%). ¹H NMR (CDCl₃, 400 MHz): δ = 9.92 (s, 1H), 7.74 (d, *J* = 4.0 Hz, 1H), 7.40 (d, *J* = 4.4 Hz, 1H), 7.28 (d, *J* = 4.0 Hz, 1H), 7.21 (d, *J* = 3.6 Hz, 1H), 7.11 (t, *J* = 4.4 Hz, 1H), 2.99 (t, *J* = 7.8 Hz, 2H), 2.94 (t, *J* = 7.8 Hz, 2H), 1.84–1.75 (m, 4H), 1.45–1.32 (m, 12H), 0.90–0.84 ppm (m, 6H).

5-[4,4'-Dihexyl-5'-(thiophen-2-yl)-2,2'-bithiazol-5-yl]furan-2-carbaldehyde (3): The synthetic method resembled that of compound **2**, and the compound was purified by column chromatography on silica gel (PE/CH₂Cl₂ = 2:1–1:1, v/v) to give an orange solid (130 mg, yield 90%). ¹H NMR (CDCl₃, 400 MHz): δ = 9.68 (s, 1H), 7.40 (d, *J* = 5.2 Hz, 1H), 7.34 (d, *J* = 4.0 Hz, 1H), 7.21 (d, *J* = 4.0 Hz, 1H), 7.11 (t, *J* = 4.4 Hz, 1H), 6.71 (d, *J* = 3.6 Hz, 1H), 3.04 (t, *J* = 7.8 Hz, 2H), 2.94 (t, *J* = 7.8 Hz, 2H), 1.84–1.75 (m, 4H), 1.48–1.28 (m, 12H), 0.91–0.88 ppm (m, 6H).

4-[4,4'-Dihexyl-5'-(thiophen-2-yl)-2,2'-bithiazol-5-yl]benzaldehyde (4): The synthetic method resembled that of compound **2**, and the compound was purified by column chromatography on silica gel (PE/CH₂Cl₂ = 3:1–1:1, v/v) to give a yellow solid (320 mg, yield 91%). ¹H NMR (CDCl₃, 400 MHz): δ = 10.07 (s, 1H), 7.96 (d, *J* = 8.4 Hz, 2H), 7.64 (d, *J* = 8.0 Hz, 2H), 7.39 (d, *J* = 5.2 Hz, 1H), 7.21 (d, *J* = 3.6 Hz, 1H), 7.11 (t, *J* = 4.4 Hz, 1H), 3.04 (t, *J* = 7.8 Hz, 2H), 2.94 (t, *J* = 7.8 Hz, 2H), 1.84–1.75 (m, 4H), 1.48–1.28 (m, 12H), 0.91–0.88 ppm (m, 6H).

5-[5'-(5-Bromothiophen-2-yl)-4,4'-dihexyl-2,2'-bithiazol-5-yl]thiophene-2-carbaldehyde (5): Compound **2** (200 mg, 0.38 mmol) and *N*-bromosuccinimide (68 mg, 0.38 mmol) were placed in a flask, and then chloroform

(8 mL) was injected under an argon atmosphere. After heating the reaction mixture at reflux for 3 h, the product was cooled to room temperature and poured into water (20 mL). The mixture was extracted with CH₂Cl₂ (3 × 20 mL). The combined organic layers were dried with anhydrous Na₂SO₄. The solvent was evaporated, and the residue was purified by column chromatography on silica gel (PE/CH₂Cl₂ = 3:1–1:1, v/v) to give a red solid (200 mg, yield 87%). ¹H NMR (CDCl₃, 400 MHz): δ = 9.92 (s, 1H), 7.40 (d, *J* = 4.0 Hz, 1H), 7.28 (d, *J* = 4.0 Hz, 1H), 7.06 (d, *J* = 4.0 Hz, 1H), 6.95 (d, *J* = 3.6 Hz, 1H), 2.99 (t, *J* = 7.8 Hz, 2H), 2.89 (t, *J* = 7.8 Hz, 2H), 1.82–1.75 (m, 4H), 1.46–1.28 (m, 12H), 0.91–0.88 ppm (m, 6H).

5-[5'-(5-Bromothiophen-2-yl)-4,4'-dihexyl-2,2'-bithiazol-5-yl]furan-2-carbaldehyde (6): The synthetic method resembled that of compound **5**, and the compound was purified by column chromatography on silica gel (PE/CH₂Cl₂ = 3:1–1:1, v/v) to give an orange solid (147 mg, yield 98%). ¹H NMR (CDCl₃, 400 MHz): δ = 9.68 (s, 1H), 7.34 (d, *J* = 3.6 Hz, 1H), 7.06 (d, *J* = 3.6 Hz, 1H), 6.95 (d, *J* = 3.6 Hz, 1H), 6.71 (d, *J* = 3.6 Hz, 1H), 3.03 (t, *J* = 7.8 Hz, 2H), 2.89 (t, *J* = 7.8 Hz, 2H), 1.82–1.76 (m, 4H), 1.46–1.30 (m, 12H), 0.91–0.88 ppm (m, 6H).

4-[5'-(5-Bromothiophen-2-yl)-4,4'-dihexyl-2,2'-bithiazol-5-yl]benzaldehyde (7): The synthetic method resembled that of compound **5**, and the compound was purified by column chromatography on silica gel (PE/CH₂Cl₂ = 2:1–1:1, v/v) to give a yellow solid (350 mg, yield 97%). ¹H NMR (CDCl₃, 400 MHz): δ = 10.07 (s, 1H), 7.96 (d, *J* = 8.4 Hz, 2H), 7.64 (d, *J* = 8.0 Hz, 2H), 7.06 (d, *J* = 4.0 Hz, 1H), 6.95 (d, *J* = 4.0 Hz, 1H), 2.89 (t, *J* = 7.8 Hz, 2H), 2.85 (t, *J* = 7.8 Hz, 2H), 1.81–1.73 (m, 4H), 1.42–1.26 (m, 12H), 0.91–0.84 ppm (m, 6H).

5-(5'-[5-[4-(Diphenylamino)phenyl]thiophen-2-yl]-4,4'-dihexyl-2,2'-bithiazol-5-yl)thiophene-2-carbaldehyde (8): Compound **5** (120 mg, 0.20 mmol), [Pd(PPh₃)₄] (22 mg, 0.02 mmol), and K₂CO₃ (1.02 g, 0.01 mol) in THF (10 mL) and H₂O (5 mL) were heated to 45°C under an argon atmosphere for 30 min. A solution of 4-(diphenylamino)phenylboronic acid (57 mg, 0.38 mmol) in THF (3 mL) was added slowly, and the mixture was heated at reflux for a further 2 h. After cooling to room temperature, THF was evaporated and the mixture was extracted with CH₂Cl₂ (3 × 20 mL). The combined organic layers were dried with anhydrous Na₂SO₄. The solvent was evaporated, and the residue was purified by column chromatography on silica gel (PE/CH₂Cl₂ = 1:1, v/v) to give a red solid (120 mg, yield 79%). ¹H NMR (CDCl₃, 400 MHz): δ = 9.92 (s, 1H), 7.74 (d, *J* = 4.0 Hz, 1H), 7.47 (d, *J* = 8.4 Hz, 2H), 7.30–7.27 (m, 5H), 7.20 (d, *J* = 3.6 Hz, 1H), 7.16 (d, *J* = 4.0 Hz, 1H), 7.13 (d, *J* = 7.6 Hz, 4H), 7.09–7.04 (m, 4H), 3.00 (t, *J* = 4.0 Hz, 2H), 2.98 (t, *J* = 4.2 Hz, 2H), 1.85–1.77 (m, 4H), 1.46–1.32 (m, 12H), 0.91–0.88 ppm (m, 6H).

5-(5'-[5-[4-(Diphenylamino)phenyl]thiophen-2-yl]-4,4'-dihexyl-2,2'-bithiazol-5-yl)furan-2-carbaldehyde (9): The synthetic method resembled that of compound **8**, and the compound was purified by column chromatography on silica gel (PE/CH₂Cl₂ = 1:1, v/v) to give a red solid (130 mg, yield 98%). ¹H NMR (CDCl₃, 400 MHz): δ = 9.68 (s, 1H), 7.47 (d, *J* = 8.8 Hz, 2H), 7.34 (d, *J* = 4.0 Hz, 1H), 7.29 (d, *J* = 8.4 Hz, 3H), 7.20 (d, *J* = 3.6 Hz, 1H), 7.16–7.12 (m, 6H), 7.09–7.04 (m, 4H), 6.71 (d, *J* = 3.6 Hz, 1H), 3.04 (t, *J* = 7.8 Hz, 2H), 3.00 (t, *J* = 7.8 Hz, 2H), 1.85–1.77 (m, 4H), 1.46–1.30 (m, 12H), 0.89 ppm (t, *J* = 7.0 Hz, 6H).

4-(5'-[5-[4-(Diphenylamino)phenyl]thiophen-2-yl]-4,4'-dihexyl-2,2'-bithiazol-5-yl)benzaldehyde (10): The synthetic method resembled that of compound **8**, and the compound was purified by column chromatography on silica gel (PE/CH₂Cl₂ = 1:1, v/v) to give an orange solid (200 mg, yield 97%). ¹H NMR (CDCl₃, 400 MHz): δ = 10.06 (s, 1H), 7.96 (d, *J* = 8.4 Hz, 2H), 7.64 (d, *J* = 8.0 Hz, 2H), 7.47 (d, *J* = 8.8 Hz, 2H), 7.29 (d, *J* = 8.0 Hz, 2H), 7.20 (d, *J* = 3.6 Hz, 1H), 7.16–7.12 (m, 5H), 7.09–7.04 (m, 5H), 6.71 (d, *J* = 3.6 Hz, 1H), 2.98 (t, *J* = 7.8 Hz, 2H), 2.85 (t, *J* = 7.8 Hz, 2H), 1.85–1.75 (m, 4H), 1.37–1.26 (m, 12H), 0.90–0.85 ppm (m, 6H).

2-Cyano-3-[5-(5'-[4-(diphenylamino)phenyl]thiophen-2-yl)-4,4'-dihexyl-2,2'-bithiazol-5-yl]thiophen-2-yl]acrylic acid (BT-I): Compound **8** (120 mg, 0.16 mmol), 2-cyanoacetic acid (93 mg, 1.09 mmol), ammonium acetate (50 mg), and acetic acid (8 mL) were heated at 120°C under an argon atmosphere for 6 h. After cooling to room temperature, the mixture was added to water. The precipitate was isolated by filtration and washed with water. The residue was purified by column chromatography

on silica gel ($\text{CH}_2\text{Cl}_2\text{-CH}_2\text{Cl}_2/\text{EtOH}=10:1$, v/v) to give a dark red solid (110 mg, yield 85%). $^1\text{H NMR}$ ($[\text{D}_6]\text{DMSO}$, 400 MHz): $\delta=8.30$ (s, 1H), 7.88 (d, $J=4.0$ Hz, 1H), 7.58 (d, $J=8.0$ Hz, 2H), 7.54 (d, $J=4.0$ Hz, 1H), 7.46 (d, $J=4.0$ Hz, 1H), 7.37–7.32 (m, 5H), 7.12–7.05 (m, 6H), 6.97 (d, $J=8.0$ Hz, 2H), 2.98–2.92 (m, 4H), 1.76–1.72 (m, 4H), 1.41–1.28 (m, 12H), 0.87–0.84 ppm (m, 6H); $^{13}\text{C NMR}$ ($[\text{D}_8]\text{THF}$, 100 MHz): $\delta=156.3$, 153.9, 147.7, 147.4, 133.6, 132.6, 131.0, 129.2, 128.7, 127.5, 126.3, 124.6, 123.2, 123.1, 122.9, 31.7, 30.9, 30.4, 29.7, 29.2, 29.0, 28.9, 22.6, 13.5 ppm; HRMS: m/z calcd for $\text{C}_{48}\text{H}_{45}\text{N}_4\text{O}_2\text{S}_4$: 837.2425 $[\text{M}-\text{H}]^-$; found: 837.2420; elemental analysis calcd (%) for $\text{C}_{48}\text{H}_{46}\text{N}_4\text{O}_2\text{S}_4$: C 68.70, H 5.53, N 6.68; found: C 68.60, H 5.62, N 6.72.

2-Cyano-3-[5-(5'-[4-(diphenylamino)phenyl]thiophen-2-yl)-4,4'-dihexyl-2,2'-bithiazol-5-yl]furan-2-yl]acrylic acid (BT-II): A procedure similar to that for the dye **BT-I**, but with compound **9** (120 mg, 0.17 mmol) instead of compound **8**, was performed to give **BT-II** as dark red solid (110 mg, yield 87%). $^1\text{H NMR}$ ($[\text{D}_6]\text{DMSO}$, 400 MHz): $\delta=8.04$ (s, 1H), 7.58 (d, $J=8.0$ Hz, 3H), 7.46 (d, $J=4.0$ Hz, 1H), 7.38–7.32 (m, 5H), 7.20 (d, $J=4.0$ Hz, 1H), 7.12–7.05 (m, 6H), 6.97 (d, $J=8.0$ Hz, 2H), 3.04 (t, $J=8.0$ Hz, 2H), 2.95 (t, $J=8.0$ Hz, 2H), 1.77–1.68 (m, 4H), 1.38–1.26 (m, 12H), 0.85 ppm (t, $J=8.0$ Hz, 6H); $^{13}\text{C NMR}$ ($[\text{D}_8]\text{THF}$, 100 MHz): $\delta=159.0$, 156.5, 154.1, 149.1, 147.8, 147.4, 145.3, 129.2, 127.5, 126.3, 124.5, 123.2, 123.0, 122.8, 111.8, 31.8, 31.7, 30.7, 30.4, 29.7, 29.1, 28.9, 28.6, 22.6, 13.5 ppm; HRMS: m/z calcd for $\text{C}_{48}\text{H}_{45}\text{N}_4\text{O}_3\text{S}_3$: 821.2654 $[\text{M}-\text{H}]^-$; found: 821.2627; elemental analysis calcd (%) for $\text{C}_{48}\text{H}_{46}\text{N}_4\text{O}_3\text{S}_3$: C 70.04, H 5.63, N 6.81; found: C 70.11, H 5.59, N 6.73.

2-Cyano-3-[4-(5'-[4-(diphenylamino)phenyl]thiophen-2-yl)-4,4'-dihexyl-2,2'-bithiazol-5-yl]phenyl]acrylic acid (BT-III): A procedure similar to that for the dye **BT-I**, but with compound **10** (120 mg, 0.17 mmol) instead of compound **8**, was performed to give **BT-III** as a red solid (190 mg, yield 88%). $^1\text{H NMR}$ ($[\text{D}_6]\text{DMSO}$, 400 MHz): $\delta=8.25$ (s, 1H), 8.09 (d, $J=8.0$ Hz, 2H), 7.70 (d, $J=8.0$ Hz, 2H), 7.57 (d, $J=8.4$ Hz, 2H), 7.43 (d, $J=3.6$ Hz, 1H), 7.35–7.31 (m, 5H), 7.11–7.05 (m, 6H), 6.97 (d, $J=8.8$ Hz, 2H), 2.93 (t, $J=7.4$ Hz, 2H), 2.82 (t, $J=7.4$ Hz, 2H), 1.77–1.67 (m, 4H), 1.39–1.23 (m, 12H), 0.86–0.81 ppm (m, 6H); $^{13}\text{C NMR}$ ($[\text{D}_6]\text{DMSO}$, 100 MHz): $\delta=163.1$, 157.9, 156.3, 154.7, 153.6, 147.2, 146.7, 144.6, 132.9, 130.8, 129.8, 129.6, 129.5, 129.4, 127.8, 126.6, 126.5, 124.4, 123.7, 123.6, 122.7, 30.9, 29.8, 29.2, 28.8, 28.6, 28.4, 28.3, 22.0, 13.9 ppm; HRMS: m/z calcd for $\text{C}_{50}\text{H}_{47}\text{N}_4\text{O}_2\text{S}_3$: 831.2861 $[\text{M}-\text{H}]^-$; found: 831.2850; elemental analysis calcd (%) for $\text{C}_{50}\text{H}_{48}\text{N}_4\text{O}_2\text{S}_3$: C 72.08, H 5.81, N 6.72; found: C 72.15, H 5.76, N 6.68.

4-(5'-Bromo-4,4'-dihexyl-2,2'-bithiazol-5-yl)-N,N-diphenylaniline (11): 5,5'-Dibromo-4,4'-dihexyl-2,2'-bithiazole (1000 mg, 2.04 mmol), $[\text{Pd}(\text{PPh}_3)_4]$ (20 mg, 0.017 mmol), and K_2CO_3 (1.02 g, 0.01 mol) in THF (10 mL) and H_2O (5 mL) were heated to 45 °C under an argon atmosphere for 30 min. A solution of 4-(diphenylamino)phenylboronic acid (590 mg, 2.04 mmol) in THF (10 mL) was added slowly, and the mixture was heated at reflux for a further 6 h. After cooling to room temperature, the mixture was extracted with CH_2Cl_2 (3×20 mL). The combined organic layers were washed with water and brine and dried with anhydrous Na_2SO_4 . The solvent was evaporated, and the residue was purified by column chromatography on silica gel ($\text{PE}/\text{CH}_2\text{Cl}_2=3:1-2:1$, v/v) to give a yellow solid (600 mg, yield 45%). $^1\text{H NMR}$ (CDCl_3 , 400 MHz): $\delta=7.31-7.21$ (m, 6H), 7.15 (d, $J=8.0$ Hz, 4H), 7.10–7.05 (m, 4H), 2.80 (t, $J=8.0$ Hz, 2H), 2.76 (t, $J=8.0$ Hz, 2H), 1.78–1.68 (m, 4H), 1.36–1.27 (m, 12H), 0.91–0.85 ppm (m, 6H).

5'-[4-(Diphenylamino)phenyl]-4,4'-dihexyl-2,2'-bithiazole-5-carbaldehyde (12): A solution of *n*BuLi (2.5 M, 0.48 mL, 1.2 mmol) in hexane was added to a solution of **11** (650 mg, 1 mmol) in THF (20 mL) at -78°C . After stirring for 1 h, a solution of *N*-formylmorpholine (172 mg, 1.5 mmol) in THF (5 mL) was added. After additional stirring for 1 h at -78°C , the mixture was allowed to warm to room temperature overnight. The final solution was acidified with 1 M HCl solution (10 mL) and stirred for 45 min at room temperature. The aqueous phase was extracted with dichloromethane, and the organic layer was dried over magnesium sulfate. After evaporation of the solvent, the final crude product was purified by column chromatography on silica gel ($\text{PE}/\text{CH}_2\text{Cl}_2=1:1$, v/v) to yield an orange solid (350 mg, yield 58%). $^1\text{H NMR}$ (CDCl_3 , 400 MHz): $\delta=10.03$ (s, 1H), 7.24–7.19 (m, 6H), 7.08 (d, $J=8.0$ Hz, 4H), 7.01 (t, $J=$

8.0 Hz, 4H), 3.02 (t, $J=8.0$ Hz, 2H), 2.77 (t, $J=8.0$ Hz, 2H), 1.78–1.66 (m, 4H), 1.27–1.19 (m, 12H), 0.83–0.78 ppm (m, 6H).

2-(4-Bromophenyl)-3-[5'-[4-(diphenylamino)phenyl]-4,4'-dihexyl-2,2'-bithiazol-5-yl]acrylonitrile (13): A mixture of compound **12** (350 mg, 0.58 mmol), 2-(4-bromophenyl)acetonitrile (117 mg, 0.60 mmol), a catalytic amount of potassium *tert*-butoxide, and methanol (20 mL) was placed in a three-neck round-bottomed flask (100 mL). After the mixture was heated at reflux for 3 h, the product was isolated by filtration and dried. The final crude product was purified by column chromatography on silica gel ($\text{PE}/\text{CH}_2\text{Cl}_2=3:2$, v/v) to yield an orange solid (400 mg, yield 88%). $^1\text{H NMR}$ (CDCl_3 , 400 MHz): $\delta=7.66$ (s, 1H), 7.59 (d, $J=8.0$ Hz, 2H), 7.52 (d, $J=8.0$ Hz, 2H), 7.30 (t, $J=8.0$ Hz, 6H), 7.16 (d, $J=8.0$ Hz, 4H), 7.11–7.06 (m, 4H), 2.93 (t, $J=8.0$ Hz, 2H), 2.84 (t, $J=8.0$ Hz, 2H), 1.83–1.74 (m, 4H), 1.39–1.27 (m, 12H), 0.90–0.87 ppm (m, 6H).

3-[5'-[4-(Diphenylamino)phenyl]-4,4'-dihexyl-2,2'-bithiazol-5-yl]-2-[4-(5-formylthiophen-2-yl)phenyl]acrylonitrile (14): Compound **13** (160 mg, 0.20 mmol), $[\text{Pd}(\text{PPh}_3)_4]$ (20 mg, 0.017 mmol), and K_2CO_3 (1.02 g, 0.01 mol) in THF (10 mL) and H_2O (5 mL) were heated to 45 °C under an argon atmosphere for 30 min. A solution of 5-formylthiophen-2-ylboronic acid (34 mg, 0.22 mmol) in THF (5 mL) was added slowly, and the mixture was heated at reflux for a further 2 h. After cooling to room temperature, the mixture was extracted with CH_2Cl_2 (3×20 mL). The combined organic layers were washed with water and brine and dried with anhydrous Na_2SO_4 . The solvent was evaporated, and the residue was purified by column chromatography on silica gel ($\text{PE}/\text{CH}_2\text{Cl}_2=1:2$, v/v) to give a red solid (130 mg, yield 78%). $^1\text{H NMR}$ (CDCl_3 , 400 MHz): $\delta=9.92$ (s, 1H), 7.81–7.72 (m, 6H), 7.53–7.47 (m, 1H), 7.33–7.28 (m, 6H), 7.17–7.07 (m, 8H), 2.96 (t, $J=8.0$ Hz, 2H), 2.85 (t, $J=8.0$ Hz, 2H), 1.81–1.62 (m, 4H), 1.42–1.31 (m, 12H), 0.91–0.78 ppm (m, 6H); HRMS: m/z calcd for $\text{C}_{50}\text{H}_{49}\text{N}_4\text{SO}_3$: 817.3069 $[\text{M}+\text{H}]^+$; found: 817.3095.

3-[5'-[4-(Diphenylamino)phenyl]-4,4'-dihexyl-2,2'-bithiazol-5-yl]-2-[4-(5-formylfuran-2-yl)phenyl]acrylonitrile (15): Compound **13** (100 mg, 0.13 mmol), $[\text{Pd}(\text{PPh}_3)_4]$ (20 mg, 0.017 mmol), and K_2CO_3 (1.02 g, 0.01 mol) in THF (10 mL) and H_2O (5 mL) were heated to 45 °C under an argon atmosphere for 30 min. A solution of 5-formylfuran-2-ylboronic acid (21 mg, 0.15 mmol) in THF (5 mL) was added slowly, and the mixture was heated at reflux for a further 2 h. After cooling to room temperature, the mixture was extracted with CH_2Cl_2 (3×20 mL). The combined organic layers were washed with water and brine and dried with anhydrous Na_2SO_4 . The solvent was evaporated, and the residue was purified by column chromatography on silica gel ($\text{PE}/\text{CH}_2\text{Cl}_2=1:3$, v/v) to give a red solid (80 mg, yield 78%). $^1\text{H NMR}$ (CDCl_3 , 400 MHz): $\delta=9.69$ (s, 1H), 7.96–7.90 (m, 2H), 7.74 (d, $J=12.0$ Hz, 3H), 7.36–7.28 (m, 7H), 7.17–7.05 (m, 8H), 6.96–6.92 (m, 1H), 2.98–2.71 (m, 4H), 1.84–1.76 (m, 4H), 1.34–1.26 (m, 12H), 0.91–0.87 ppm (m, 6H); HRMS: m/z calcd for $\text{C}_{50}\text{H}_{49}\text{N}_4\text{S}_2\text{O}_2$: 801.3297 $[\text{M}+\text{H}]^+$; found: 801.3290.

3-[5'-[4-(Diphenylamino)phenyl]-4,4'-dihexyl-2,2'-bithiazol-5-yl]-2-(4'-formylbiphenyl-4-yl)acrylonitrile (16): Compound **13** (130 mg, 0.17 mmol), $[\text{Pd}(\text{PPh}_3)_4]$ (20 mg, 0.017 mmol), and K_2CO_3 (1.02 g, 0.01 mol) in THF (10 mL) and H_2O (5 mL) were heated to 45 °C under an argon atmosphere for 30 min. A solution of 4-formylphenylboronic acid (30 mg, 0.20 mmol) in THF (5 mL) was added slowly, and the mixture was heated at reflux for a further 2 h. After cooling to room temperature, the mixture was extracted with CH_2Cl_2 (3×20 mL). The combined organic layers were washed with water and brine and dried with anhydrous Na_2SO_4 . The solvent was evaporated, and the residue was purified by column chromatography on silica gel ($\text{PE}/\text{CH}_2\text{Cl}_2=1:2$, v/v) to give a red solid (110 mg, yield 78%). $^1\text{H NMR}$ (CDCl_3 , 400 MHz): $\delta=10.08$ (s, 1H), 8.01–7.98 (m, 2H), 7.84–7.73 (m, 7H), 7.33–7.28 (m, 6H), 7.17–7.07 (m, 8H), 2.98–2.71 (m, 4H), 1.84–1.76 (m, 4H), 1.42–1.31 (m, 12H), 0.92–0.85 ppm (m, 6H); HRMS: m/z calcd for $\text{C}_{52}\text{H}_{51}\text{N}_4\text{SO}_2$: 811.3504 $[\text{M}+\text{H}]^+$; found: 811.3522.

2-Cyano-3-[5-[4-(1-cyano-2-[5'-[4-(diphenylamino)phenyl]-4,4'-dihexyl-2,2'-bithiazol-5-yl]vinyl)phenyl]thiophen-2-yl]acrylic acid (BT-IV): Compound **14** (130 mg, 0.16 mmol), 2-cyanoacetic acid (93 mg, 1.09 mmol), ammonium acetate (50 mg), and acetic acid (8 mL) were heated at 120 °C for 4 h. After cooling to room temperature, the mixture was added to water. The precipitate was isolated by filtration and washed with water.

The residue was purified by column chromatography on silica gel (CH_2Cl_2 - $\text{CH}_2\text{Cl}_2/\text{EtOH}=5:1$, v/v) to give a red solid (120 mg, yield 93%). $^1\text{H NMR}$ ($[\text{D}_8]\text{THF}$, 400 MHz): $\delta=8.41$ (s, 1H), 7.96–7.86 (m, 3H), 7.75–7.57 (m, 4H), 7.40–7.25 (m, 6H), 7.14–7.03 (m, 8H), 3.04 (d, $J=8.0$ Hz, 2H), 2.94 (d, $J=8.0$ Hz, 2H), 1.82–1.76 (m, 4H), 1.36–1.29 (m, 12H), 0.93–0.87 ppm (m, 6H); $^{13}\text{C NMR}$ ($[\text{D}_8]\text{THF}$, 100 MHz): $\delta=165.2$, 160.3, 153.2, 147.5, 142.8, 136.7, 134.4, 129.4, 128.5, 128.0, 127.8, 127.1, 126.4, 124.9, 123.5, 122.2, 117.2, 105.9, 88.6, 78.3, 78.0, 31.9, 30.4, 29.8, 29.6, 29.4, 28.9, 28.8, 22.8, 22.7, 14.2 ppm; HRMS: m/z calcd for $\text{C}_{53}\text{H}_{46}\text{N}_5\text{O}_2\text{S}_2$: 882.2970 $[\text{M}-\text{H}]^+$; found: 882.2976; elemental analysis calcd (%) for $\text{C}_{53}\text{H}_{46}\text{N}_5\text{O}_2\text{S}_2$: C 71.99, H 5.59, N 7.92; found: C 72.07, H 5.49, N 7.86.

2-Cyano-3-[5-[4-(1-cyano-2-[5'-[4-(diphenylamino)phenyl]-4,4'-dihexyl-2,2'-bithiazol-5-yl]vinyl)phenyl]furan-2-yl]acrylic acid (BT-V): A procedure similar to that for the dye BT-IV, but with compound 15 (80 mg, 0.10 mmol) instead of compound 14, was performed to give BT-V as a red solid (80 mg, yield 92%). $^1\text{H NMR}$ ($[\text{D}_8]\text{THF}$, 400 MHz): $\delta=8.35$ (s, 1H), 7.91–7.80 (m, 4H), 7.63–7.47 (m, 3H), 7.22–7.14 (m, 6H), 7.06–6.92 (m, 8H), 3.05 (d, $J=8.0$ Hz, 2H), 2.84 (d, $J=8.0$ Hz, 2H), 1.83–1.78 (m, 4H), 1.40–1.26 (m, 12H), 0.92–0.86 ppm (m, 6H); $^{13}\text{C NMR}$ ($[\text{D}_8]\text{THF}$, 100 MHz): $\delta=164.5$, 160.8, 154.5, 147.9, 143.8, 137.2, 135.0, 132.4, 129.5, 128.4, 128.2, 127.6, 127.2, 126.6, 124.5, 123.4, 123.2, 117.2, 106.2, 90.6, 78.6, 78.3, 32.1, 30.9, 29.8, 29.7, 29.5, 29.4, 28.9, 28.6, 28.2, 22.9, 22.5, 13.8 ppm; HRMS: m/z calcd for $\text{C}_{53}\text{H}_{46}\text{N}_5\text{O}_2\text{S}_2$: 866.3199 $[\text{M}-\text{H}]^+$; found: 866.3185; elemental analysis calcd (%) for $\text{C}_{53}\text{H}_{46}\text{N}_5\text{O}_2\text{S}_2$: C 73.33, H 5.69, N 8.07; found: C 73.40, H 5.78, N 8.15.

2-Cyano-3-[4'-(1-cyano-2-[5'-[4-(diphenylamino)phenyl]-4,4'-dihexyl-2,2'-bithiazol-5-yl]vinyl)biphenyl-4-yl]acrylic acid (BT-VI): A procedure similar to that for the dye BT-IV, but with compound 16 (120 mg, 0.15 mmol) instead of compound 14, was performed to give BT-VI as a red solid (110 mg, yield 85%). $^1\text{H NMR}$ ($[\text{D}_8]\text{THF}$, 400 MHz): $\delta=8.31$ (s, 1H), 8.18 (d, $J=4.0$ Hz, 2H), 8.02 (s, 1H), 7.96–7.89 (m, 6H), 7.39–7.25 (m, 6H), 7.14–7.03 (m, 9H), 3.05 (d, $J=8.0$ Hz, 2H), 2.72 (d, $J=8.0$ Hz, 2H), 1.86–1.78 (m, 4H), 1.44–1.28 (m, 12H), 0.93–0.87 ppm (m, 6H); $^{13}\text{C NMR}$ ($[\text{D}_8]\text{THF}$, 100 MHz): $\delta=164.2$, 161.8, 154.2, 147.3, 140.0, 135.9, 131.4, 129.9, 129.3, 128.3, 127.5, 127.2, 126.4, 124.9, 123.5, 122.2, 117.2, 109.5, 78.6, 78.3, 78.0, 31.7, 31.6, 29.7, 29.6, 29.5, 29.1, 28.9, 22.6, 22.5, 13.5 ppm; HRMS: m/z calcd for $\text{C}_{55}\text{H}_{50}\text{N}_5\text{O}_2\text{S}_2$: 876.3406 $[\text{M}-\text{H}]^+$; found: 876.3406; elemental analysis calcd (%) for $\text{C}_{55}\text{H}_{50}\text{N}_5\text{O}_2\text{S}_2$: C 75.22, H 5.85, N 7.98; found: C 75.13, H 5.93, N 7.87.

Materials and reagents: Tetrahydrofuran (THF) was predried over 4 Å molecular sieves and distilled under an argon atmosphere from sodium benzophenone ketyl immediately prior to use. Dichloromethane was distilled under normal pressure and dried over calcium hydroxide. 5,5'-Di-bromo-4,4'-dihexyl-2,2'-bithiazole and 1-propyl-3-methylimidazolium iodide (PMII) were prepared according to published procedures.^[30] Methoxypropionitrile (MPN) and 1,2-dimethyl-3-*n*-propylimidazolium iodide (DMPII) were purchased from Aldrich. Benzimidazole (BI) was from J&K. Tetra-*n*-butylammonium hexafluorophosphate (TBAPF_6), 4-*tert*-butylpyridine (TBP), and lithium iodide were from Fluka and iodine (99.999%) was from Alfa Aesar. Transparent fluorine-doped tin oxide (FTO) conducting glass (transmission >90% in the visible, sheet resistance $15 \Omega\text{square}^{-1}$) was obtained from the Geao Science and Educational Co. Ltd. of China. All other solvents and chemicals used in this work were of reagent grade and used without further purification unless otherwise noted.

Characterization: ^1H and ^{13}C NMR spectra were recorded on Brücker AM 400 MHz instruments with tetramethylsilane as the internal standard. HRMS was performed with a Waters LCT Premier XE spectrometer. The absorption spectra of sensitizer dyes in solution and adsorbed on TiO_2 films were measured with a Varian Cary 500 spectrophotometer. Emission spectra of sensitized dyes in solution were measured with a Varian Cary Eclipse spectrometer. Cyclic voltammograms were determined with a Versastat II electrochemical workstation (Princeton Applied Research) by using a three-electrode cell with a Pt working electrode, a Pt wire counter electrode, and a saturated calomel reference electrode in saturated KCl solution; 0.1 M tetrabutylammonium hexafluorophosphate (TBAPF_6) was used as the supporting electrolyte in

THF. The ferrocene/ferrocenium (Fc/Fc^+) redox couple was used as an internal potential reference.

Device fabrication: The TiO_2 films were fabricated with a screen-printing method according to the published procedure.^[18b] The thickness was about 15 μm . The trilayer TiO_2 electrodes were heated under an air flow at 450 °C for 15 min and 500 °C for 15 min. The sintered films were further treated with 40 mM TiCl_4 aqueous solution at room temperature for 12 h and washed with water and ethanol, which significantly increased the short-circuit photocurrent. Aqueous TiCl_4 removed the iron contamination source, which can quench the dye-sensitized photocurrent (J_{sc}) effectively.^[31] Then, the films were annealed at 450 °C for 30 min. After the TiCl_4 -pretreated films were cooled to around 50 °C, they were immersed in a 3×10^{-4} M dye bath in CH_2Cl_2 solution and maintained in the dark for 18 h at room temperature. The electrodes were then rinsed with CH_2Cl_2 and ethanol and dried. The size of the TiO_2 electrodes used was 0.25 cm^2 . To prepare the counter electrode, a Pt catalyst was deposited on cleaned FTO glass by spinning with a drop of H_2PtCl_6 solution (20 mM 2-propanol solution) with heat treatment at 400 °C for 15 min. A hole (0.6 mm diameter) was drilled on the counter electrode using a drill press. The perforated sheet was cleaned with ultrasound in an ethanol bath for 10 min. For the assembly of DSSCs, the dye-covered TiO_2 electrode and Pt counter electrode were assembled into a sandwich-type cell and sealed with a hot-melt gasket of thickness 25 μm made of the ionomer Surlyn 1702 (DuPont). The electrolyte was introduced into the cell by vacuum back-filling from a hole in the back of the counter electrode. Finally, the hole was sealed with a self-adhesive silver film. In this work, two kinds of electrolyte were employed: liquid electrolyte comprising 0.1 M LiI, 0.05 M I_2 , 0.6 M DMPII, and 0.5 M TBP in a mixture of acetonitrile and methoxypropionitrile (volume ratio, 7:3); and ionic-liquid electrolyte comprising 0.1 M LiI, 0.1 M I_2 , and 0.45 M benzimidazole in 1-methyl-3-*n*-propylimidazolium iodide (MPII).

Photovoltaic performance measurements: Photovoltaic measurements employed an AM 1.5 solar simulator equipped with a 300 W xenon lamp (Model No. 91160, Oriel). The power of the simulated light was calibrated to 100 mWcm^{-2} by using a Newport Oriel PV reference cell system (Model 91150 V). J - V curves were obtained by applying an external bias to the cell and measuring the generated photocurrent with a Keithley model 2400 digital source meter. The voltage step and delay time of the photocurrent were 10 mV and 40 ms, respectively. Action spectra of the incident monochromatic photon-to-electron conversion efficiency (IPCE) for the solar cells were obtained with a Newport-74125 system (Newport Instruments). The intensity of monochromatic light was measured with a Si detector (Newport-71640).

Acknowledgements

This work was supported by NSFC/China (2116110444, 21172073, and 61006048), the National Basic Research 973 Program (2011CB808400), the Fundamental Research Funds for the Central Universities (WJ0913001), the Ph.D. Programs Foundation of the Ministry of Education of China (20090074110004), and the Scientific Committee of Shanghai (10520709700). We are grateful to Dr. Xin Li in the Department of Theoretical Chemistry and Biology, School of Biotechnology, KTH Royal Institute of Technology in Sweden for computational assistance.

- [1] B. O'Regan, M. Grätzel, *Nature* **1991**, 353, 737–740.
- [2] a) F. Gao, Y. Wang, J. Zhang, D. Shi, M. Wang, R. Humphry-Baker, P. Wang, S. M. Zakeeruddin, M. Grätzel, *Chem. Commun.* **2008**, 2635–2637; b) J. H. Yum, I. Jung, C. Baik, J. Ko, M. K. Nazeeruddin, M. Grätzel, *Energy Environ. Sci.* **2009**, 2, 100–102.
- [3] A. Mishra, M. K. Fischer, P. Bauerle, *Angew. Chem.* **2009**, 121, 2510–2536; *Angew. Chem. Int. Ed.* **2009**, 48, 2474–2499.
- [4] a) K. Sayama, K. Hara, Y. Ohga, A. Shinpou, S. Suga, H. Arakawa, *New J. Chem.* **2001**, 25, 200–202; b) X. M. Ma, J. L. Hua, W. J. Wu, H. Tian, *Tetrahedron* **2008**, 64, 345–350; c) J. Tang, W. J. Wu, J. L.

- Hua, J. Li, H. Tian, *Energy Environ. Sci.* **2009**, *2*, 982–990; d) K. Funabiki, H. Mase, A. Hibino, N. Tanaka, N. Mizuhata, Y. Sakuragi, A. Nakashima, T. Yoshida, Y. Kubotaa, M. Matsui, *Energy Environ. Sci.* **2011**, *4*, 2186–2192.
- [5] a) K. Sayama, K. Hara, N. Mori, M. Satsuki, S. Suga, S. Tsukagoshi, Y. Abe, H. Sugihara, H. Arakawa, *Chem. Commun.* **2000**, 1173–1174; b) K. Sayama, S. Tsukagoshi, T. Mori, K. Hara, Y. Ohga, A. Shinpo, Y. Abe, S. Suga, H. Arakawa, *Solar Energy Mater. Solar Cells* **2003**, *80*, 47–71.
- [6] a) K. Hara, T. Sato, R. Katoh, A. Furube, Y. Ohga, A. Shinpo, S. Suga, K. Sayama, H. Sugihara, H. Arakawa, *J. Phys. Chem. A J. Phys. Chem. B* **2003**, *107*, 597–606; b) K. Hara, Z. S. Wang, T. Sato, A. Furube, R. Katoh, H. Sugihara, Y. Dan-oh, C. Kasada, A. Shinpo, S. Suga, *J. Phys. Chem. B* **2005**, *109*, 15476–15482; c) Z. S. Wang, Y. Cui, K. Hara, Y. Dan-oh, C. Kasada, A. Shinpo, *Adv. Mater.* **2007**, *19*, 1138–1141.
- [7] a) W. H. Howie, F. Claeysens, H. Miura, L. M. Peter, *J. Am. Chem. Soc.* **2008**, *130*, 1367–1375; b) D. B. Kuang, S. Uchida, R. Humphry-Baker, S. M. Zakeeruddin, M. Grätzel, *Angew. Chem.* **2008**, *120*, 1949–1953; *Angew. Chem. Int. Ed.* **2008**, *47*, 1923–1927; c) T. Dentani, Y. Kubota, K. Funabiki, J. Jin, T. Yoshida, H. Minoura, H. Miura, M. Matsui, *New J. Chem.* **2009**, *33*, 93–101; d) W. Zhu, Y. Wu, Z. S. Wang, W. Li, X. Li, J. Chen, Z. Wang, H. Tian, *Adv. Funct. Mater.* **2011**, *21*, 756–763; e) B. Liu, W. Zhu, Q. Zhang, W. Wu, M. Xu, Z. Ning, Y. Xie, H. Tian, *Chem. Commun.* **2009**, 1766–1768; f) B. Liu, W. Wu, X. Li, L. Li, S. Guo, X. Wei, W. Zhu, Q. Liu, *Phys. Chem. Chem. Phys.* **2011**, *13*, 8985–8992; g) W. Q. Li, Y. Z. Wu, X. Li, Y. S. Xie, W. H. Zhu, *Energy Environ. Sci.* **2011**, *4*, 1830–1837.
- [8] a) Z. S. Wang, F. Y. Li, C. H. Huang, *Chem. Commun.* **2000**, 2063–2064; b) E. Stathatos, P. Lianos, *Chem. Mater.* **2001**, *13*, 3888–3892.
- [9] a) H. N. Tian, X. C. Yang, R. K. Chen, Y. Z. Pan, L. Li, A. Hagfeldt, L. C. Sun, *Chem. Commun.* **2007**, 3741–3743; b) W. J. Wu, J. B. Yang, J. L. Hua, J. Tang, L. Zhang, Y. T. Long, H. Tian, *J. Mater. Chem.* **2010**, *20*, 1772–1779.
- [10] H. N. Tian, X. C. Yang, R. K. Chen, A. Hagfeldt, L. C. Sun, *Energy Environ. Sci.* **2009**, *2*, 674–677.
- [11] a) S. Qu, W. Wu, J. Hua, C. Kong, Y. Long, H. Tian, *J. Phys. Chem. C* **2010**, *114*, 1343–1349; b) F. Guo, S. Qu, W. Wu, J. Li, W. Ying, J. Hua, *Synth. Met.* **2010**, *160*, 1767–1773; c) Q. Li, L. Lu, C. Zhong, J. Huang, Q. Huang, J. Shi, X. Jin, T. Peng, J. Qin, Z. Li, *Chem. Eur. J.* **2009**, *15*, 9664–9668.
- [12] a) W. Zeng, Y. Cao, Y. Bai, Y. Wang, Y. Shi, M. Zhang, F. Wang, C. Pan, P. Wang, *Chem. Mater.* **2010**, *22*, 1915–1925; b) L. Li, Y. Hao, X. Yang, J. Zhao, H. Tian, C. Teng, A. Hagfeldt, L. Sun, *ChemSusChem* **2011**, *4*, 609–612.
- [13] Y. Numata, I. Ashraful, Y. Shirai, L. Y. Han, *Chem. Commun.* **2011**, 47, 6159–6161.
- [14] H. Choi, H. Choi, S. Paek, K. Song, M.-S. Kang, J. Ko, *Bull. Korean Chem. Soc.* **2010**, *31*, 125–132.
- [15] Y. T. Li, C. L. Chen, Y. Y. Hsu, H. C. Hsu, Y. Chi, B. S. Chen, W. H. Liu, C. H. Lai, T. Y. Lin, P. T. Chou, *Tetrahedron* **2010**, *66*, 4223–4229.
- [16] C. H. Chen, Y. C. Hsu, H. H. Chou, K. R. J. Thomas, J. T. Lin, C. P. Hsu, *Chem. Eur. J.* **2010**, *16*, 3184–3193.
- [17] L. Y. Lin, C.-H. Tsai, K.-T. Wong, T.-W. Huang, C.-C. Wu, S.-H. Chou, F. Lin, S.-H. Chenc, A.-I. Tsai, *J. Mater. Chem.* **2011**, *21*, 5950–5958.
- [18] J. He, W. Wu, J. Hua, Y. Jiang, S. Qu, J. Li, Y. Long, H. Tian, *J. Mater. Chem.* **2011**, *21*, 6054–6062.
- [19] Z. S. Wang, N. Kourmura, Y. Cui, M. Takahashi, H. Sekiguchi, A. Mori, T. Kubo, A. Furube, K. Hara, *Chem. Mater.* **2008**, *20*, 3993–4003.
- [20] a) R. Katoh, A. Furube, S. Mori, M. Miyashita, K. Sunahara, N. Kourmura, K. Hara, *Energy Environ. Sci.* **2009**, *2*, 542–546; b) U. F. Bunz, *Angew. Chem.* **2010**, *122*, 5159–5162; *Angew. Chem. Int. Ed.* **2010**, *49*, 5037–5040.
- [21] a) C. H. Woo, P. M. Beaujuge, T. W. Holcombe, O. P. Lee, J. J. Frechet, *J. Am. Chem. Soc.* **2010**, *132*, 15547–15549; b) J. C. Bijleveld, B. P. Karsten, S. J. Mathijssen, M. M. Wienk, D. M. Leeuw, R. J. Janssen, *J. Mater. Chem.* **2011**, *21*, 1600–1606.
- [22] S.-T. Huang, Y.-C. Hsu, Y.-S. Yen, H. H. Chou, J. T. Lin, C.-W. Chang, C.-P. Hsu, C. Tsai, D.-J. Yin, *J. Phys. Chem. C* **2008**, *112*, 19739–19747.
- [23] P. Wang, C. Klein, R. Humphry-Baker, S. M. Zakeeruddin, M. Grätzel, *J. Am. Chem. Soc.* **2005**, *127*, 808–809.
- [24] J. Tang, J. Hua, W. Wu, J. Li, Z. Jin, Y. Long, H. Tian, *Energy Environ. Sci.* **2010**, *3*, 1736–1745.
- [25] R. Z. Li, D. Shi, D. F. Zhou, Y. M. Cheng, G. L. Zhang, P. Wang, *J. Phys. Chem. C* **2009**, *113*, 7469–7479.
- [26] C. Teng, X. Yang, C. Yang, S. Li, M. Cheng, A. Hagfeldt, L. Sun, *J. Phys. Chem. C* **2010**, *114*, 9101–9110.
- [27] F. Fabregat-Santiago, G. Garcia-Belmonte, I. Mora-Seró, J. Bisquert, *Phys. Chem. Chem. Phys.* **2011**, *13*, 9083–9118.
- [28] L. C. Zou, C. Hunt, *J. Electrochem. Soc.* **2009**, *156*, C8–C15.
- [29] S. Y. Qu, B. Wang, F. L. Guo, J. Li, W. J. Wu, C. Kong, Y. T. Long, J. L. Hua, *Dyes Pigm.* **2012**, *92*, 1384–1393.
- [30] a) J. Lee, B. J. Jung, S. K. Lee, J. I. Lee, H. J. Cho, H. K. Shim, *J. Polym. Sci. Part A* **2005**, *43*, 1845–1857; b) P. Bonhôte, A.-P. Dias, N. Papageorgiou, K. Kalyanasundaram, M. Grätzel, *Inorg. Chem.* **1996**, *35*, 1168–1178.
- [31] S. Ito, T. N. Murakami, P. Comte, P. Liska, C. Grätzel, M. K. Nazeeruddin, M. Grätzel, *Thin Solid Films* **2008**, *516*, 4613–4619.

Received: November 24, 2011

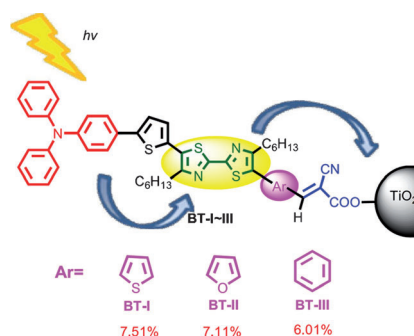
Revised: March 3, 2012

Published online: ■■■, 0000

Solar Cells

J. He, F. Guo, X. Li, W. Wu,* J. Yang,
J. Hua*

New Bithiazole-Based Sensitizers for Efficient and Stable Dye-Sensitized Solar Cells



Catch the sun: A series of dyes comprising bithiazole with a thiophene, furan, benzene, or cyano moiety as the π spacer act as the sensitizers for dye-sensitized solar cells (DSSCs, see figure). The conversion efficiencies are 3.58–7.51 %, in which **BT-I**-based DSSCs show the best photovoltaic performance under AM 1.5 irradiation. The **BT-I–III**-based DSSCs with ionic-liquid electrolytes have long-term stability and **BT-II** has up to 5.75 % power conversion efficiency.